Coronal Mass Ejections

R. S. Steinolfson

Institute for Fusion Studies

University of Texas at Austin

Austin, TX 78712

(512 471-6121)

I. Introduction

Coronal mass ejections (CMEs) are now recognized as an important component of the large-scale evolution of the solar corona. They have been observed routinely, although not continuously, since the early 1970s by white-light coronagraphs, which measure the Thomson scattering of photospheric light by coronal electrons. Time sequential images reveal coronal features since relatively bright regions contain excess mass while comparatively dark regions have less mass. Distinguishing characteristics of CMEs are the appearance of new, bright, coherent features, comparable in size to the solar diameter, in the coronagraph field of view and temporal changes on time scales of minutes to hours (Hundhausen *et al.*, 1984a). They originate near the coronal base, have a predominantly outward motion, and involve the addition of both mass and energy to the corona. They subsequently pass out of the coronagraph upper field of view and continue into interplanetary space. A considerably longer period (on the order of a day) is required for the corona to return to near its pre-event state.

CMEs were first observed about 15 years ago by the Orbiting Solar Observatory (OSO-7) white-light coronagraph (Tousey, 1973). Since then an appreciable data base has been accumulated with results from three subsequent orbiting instruments. The Skylab coronagraph operated during 1973-1974 and recorded 77 events (Munro *et al.*, 1979). This was followed by the Solwind coronagraph on the P-78 satellite, which obtained in excess of 1200 CME observations during 1979-1985 (Sheeley *et al.*, 1980). The only instrument currently operating is the coronagraph-polarimeter (C/P) on the Solar Maximum Mission (SMM) satellite. It recorded approximately 70 CMEs over a time period of a few months until it failed in 1980 but has been operational since its repair in 1984. The orbiting coronagraphs individually observe over different portions of the corona varying from a minimum of 1.6 solar radii (C/P on SMM) out to a maximum of 10 solar radii (Solwind). This data

set is supplemented by the ground-based High Altitude Observatory K-coronameter at Mauna Loa, Hawaii (Fisher and Poland, 1981), which observes the corona nearer the sun (from 1.2 to 2.0 solar radii), and by the zodiacal light photometers on the Helios spacecraft (Jackson and Leinart, 1985), which detect interplanetary transients.

Several review papers have been written on various aspects of the CME phenomena. Among the more recent and general reviews are those by Hundhausen *et al.* 1984b, Kahler (1987), and Hundhausen (1988). In addition, Kahler (1988) concentrated on observations and Steinolfson (1988) reviewed observations and theory relating to possible driving mechanisms. Some statistical properties of CMEs derived from large data sets have been discussed by MacQueen (1980), Howard *et al.* (1984), and Wagner (1984).

We will begin in the following section by reviewing some representative observations of CMEs, with emphasis on more recent results. In the remainder of the paper we concentrate on recent observations and theory as they relate to the following aspects of CMEs: (1) the role of waves in determining the white-light signature and (2) the mechanism by which the CME is driven (or launched) into the corona.

II. Observations

CMEs are observed to occur in a wide variety of sizes and shapes and at various latitudes (Munro *et al.,* 1979; Howard *et al.,* 1984). We will be primarily concerned with the subset in which the definitive leading bright signature has the appearance of a radially-expanding loop. It is not ususual for such CMEs to be associated with the equatorial streamer belt, which is the streamer "blowout" classification used by Howard *et al.* (1985). Our motivation for emphasizing the loop-shaped CME is that (a) they are a significant fraction of the total observed [20% in the Skylab data set (Sime *et al.,* 1984)

and at least 2/3 of those in the SMM data in 1980 (Hundhausen, 1988)] and (b) they are geometrically simple and , hence, are more easily studied theoretically.

A loop-like CME detected by the SMM C/P instrument is shown in Figure 1 (Hundhausen *et al.,* 1984a). CMEs are often observed to have the three-part structure displayed in the figure. That is, a preceeding bright loop followed by a dark cavity containing an additional outward moving bright structure, which in this case has the appearance of a second expanding bright loop. The dark disk is a sun-centered occulting disk that blocks out the sun. The CME had an outward velocity of about 260 km s^{-1}, which is near the low end of the observed speed range (from tens to thousands of km s^{-1}). The leading bright loop and following dark cavity are the necessary components of CMEs we will be primarily concerned with. The second bright structure may or may not be present or detectable in individual events. During 1980, it could be detected in up to 3/4 of the loop-like CMEs seen by SMM (Hundhausen, 1988). Whether or not this second structure can be located in the data as well as its shape may be due to a solar cycle effect, which is just beginning to be understood. The entire CME phenomena may also consist of waves generated beyond, or as part of, the outer bright loop. These waves often produce observable changes in nearby structures. More will be said about the role of such waves in the following section.

The loop-like CMEs of primary interest here often appear to originate near the base of, and propagate outward through, pre-existing, well-formed helmet or coronal streamers, which may be part of the equatorial streamer belt as mentioned above. The 4 loop-like Skylab CMEs studied by Sime *et al.,* (1984) and all but 1 of the 16 used in CME onset program (Harrison *et al.,* 1988) originated near the base of coronal streamers. Since difference images are used to identify CMEs in the Solwind data, it is difficult to determine the pre-event corona in this data.

Coronal streamers form over polarity inversion (neutral) lines in the radial magnetic field on the solar surface. The magnetic geometry of streamers is such that they consist of low-lying closed field lines surrounded by field lines open to the interplanetary medium. The corona flows outward along open field lines and is trapped within the closed region. Prominences tend to form within the closed-field region and also lie over local neutral lines that may be coincident with the streamer neutral line. This general picture is supported by observations indicating that CMEs can often be associated with eruptive prominences (Munro *et al.,* 1979; Webb and Hundhausen, 1987). A schematic of the initial state and the CME is shown in Figure 2. In this simplified sketch the prominence overlies the same inversion line as the streamer. Recent observations, however, using approximately simultaneous images from the SMM C/P, the MLSO Mark III K-coronameter and the MLSO prominence monitor show the eruptive prominence to often be distinctly asymmetric with respect to the CME bright loop (Hundhausen, 1988). This would indicate that the prominence may form over a local inversion line in the active region and preferentially on one side of the streamer inversion line. In addition, if a flare occurs in association with a CME, it almost invariably occurs under one leg of the expanding bright CME loop (Harrison, 1986) and generally under the loop leg closer to the equator. More will be said about the temporal and spatial relation of flares, prominences and CMEs in the section on driving mechanisms. We note here that the picture that seems to evolve from various data sets is one in which the streamer forms in a large-scale, global magnetic structure while the prominence and flare form in smaller magnetic structures imbedded in local active regions within the global field.

The characteristic three-part structure of the CME mentioned above is indicated in the schematic in Figure 2(b). The observed bright inner structure, as seen in Figure 1, has been interpreted as the eruptive prominence, and the dark cavity as the cavity originally

around the prominence. Whether or not the eruptive prominence material appears loop-like may depend partially on its orientation in the plane-of-the-sky. Waves extending beyond the bright CME loop, particularly to the sides, may also be a portion of the entire phenomena, as suggested in the model by Steinolfson (1985). If the waves steepen sufficiently, they may contribute to the bright signature. Simulations show that shock compression may be responsible for part of the increased brightness near the radial leading edge of the loop. Away from the bright loop the orientation of the wave normal to the ambient magnetic field in streamers is such that the wave produces a very small compression of the corona and probably would not be detected in coronagraphs.

III. Role of waves in CMEs

During the early analyses of CME observations, the general concensus appeared to be that the CME (in particular, the bright loop) was magnetically controlled and driven much as in the conceptual models of Kopp and Pneumann (1976) and Mouschovias and Poland (1978). The bright loop was a result of dense material carried outward from the lower corona by the expanding magnetic field. The first self-consistent MHD simulations of CMEs, on the other hand, suggested the interpretation that the bright loop resulted from shock compression of ambient coronal plasma by a fast mode MHD shock (Dryer *et al.*, 1979). The shock model has subsequently been shown to not be applicable to loop-like CMEs for several reasons, but primarily because of the observed restricted lateral motion of the loop legs that directly contradicts the model (Sime *et al.*, 1984). The expanding magnetic loop model may be conceptually correct, but this remains to be demonstrated with a quantitative self-consistent study.

Although the bright CME loop may not be entirely a result of shock compression, it is clear that waves must be involved in CMEs. The corona is a compressible medium

and the movement of a disturbance through it at typical observed CME velocities must generate a wave response. The type of wave response is governed to a large extent by the magnitude of the CME speed relative to characteristic wave velocities in the corona (or the velocities at which information can be transmitted through the corona). As mentioned above, CME speeds cover a wide range, but histograms (Gosling *et al.,* 1976; Howard *et al.,* 1985) show that typical velocities are a few hundred km s^{-1}, say 200 - 500 km s^{-1}. For a coronal temperature of 10^6 °K, the sound speed is about 170 km s^{-1}. The magnitude of the coronal magnetic field is not well known, but extrapolation of interplanetary observations gives a value of about 0.2 G at a heliocentric distance of 3 solar radii. Using a typical number density at this location implies that the Alfven speed is about 620 km s^{-1}, or that the plasma beta (β) is about 0.1. Typical CME speeds, then, are supersonic but sub-Alfvenic.

The relevant wave speeds to determine the detailed response are the slow, intermediate and fast speeds in the direction of the wave normal. The presence of the magnetic field, of course, introduces (in addition to multiple characteristic speeds) the further complication of making the corona anistropic to wave propagation. For outward propagation along a radial magnetic field and for $\beta < 1$, the slow speed becomes the sound velocity and the fast and intermediate speeds become the Alfven velocity. Hence, it is reasonable to consider the general coronal wave response in terms of the CME speed relative to the sound and Alfven speeds.

If the CME speed exceeds the fast-mode (Alfven) speed, one would expect formation of fast-mode MHD shocks. This is the situation studied in the above simulations (Dryer *et al.,* 1979), although the CME loop would generally not be associated with the shock-compressed plasma. Sime and Hundhausen (1987) have shown that for only 1 of 70 mass ejections observed with the SMM coronagraph during 1980 was there indication

that the shock produced the leading bright disturbance at all latitude locations. That is, there was no noticable disturbance of adjacent structures prior to arrival of the bright shock. This example is the exception, however, since in general there are readily observable disturbances of ambient corona structures outside the bright CME loop – particularly latitudinally displaced from the loop, although not necessarily ahead of it. Such disturbances occur although there is no observable bright structure connecting the CME loop to the disrupted feature. This behavior can be understood from the model and simulations of Steinolfson (1985) and Steinolfson and Hundhausen (1988a). They showed that when the CME velocity exceeds the fast-mode speed, a fast MHD shock does form and is coincident with the outermost part of the bright CME loop. At the flanks, however, the shock propagates away from the loop and produces the observable displacements of nearby ambient structures. Except near the top of the CME loop, the shock is a fast MHD shock propagating at small angles to the ambient (predominantly radial) magnetic field. The shock thus produces a very small density rise with its primary effects being to turn the ambient field and accelerate the corona parallel to the shock front. Consequently, the shock easily disturbs ambient structures without producing a detectable brightness increase.

For the more common example when the CME speed is supersonic and sub-Alfvenic, fast MHD shocks do not form, but slow shocks may develop. By considering the magnetic field change across slow shocks and the expected field configuration of a CME loop, Hundhausen *et al.,* (1987) suggested that such slow shocks would be concave upward as shown in Figure 3(b). The situation for a preceeding fast shock as discussed above would be as shown schematically in Figure 3(a). The authors reasoned that such a shape for the slow shock would explain the flat tops of some mass ejections, as well as the deflection of adjacent structures.

Steinolfson and Hundhausen (1988b, 1988c) used time-dependent numerical solu-

tions of the MHD equations in two-dimensions to generate wave systems propagating outward through simplified static coronas with various prescribed field geometries, uniform thermodynamics, and no gravity. For an initially radial field and disturbance speed larger than the sound and less than the Alfven velocities, a slow shock is formed as shown in Figure 4, but it is concave downward and is preceeded by a fast-mode expansion. The solution is symmetric about the left edge, and the driver was initiated at the bottom which is taken to represent the base of the corona. The authors suggested that the slow shock geometry may be a result of the fact that the field lines in this particular study are constrained to be essentially vertical behind the slow shock. Recent unpublished results show that a concave-upward shock is produced in the more realistic case of a magnetic driver inside a closed-field region in which case the field lines are bent away from the center symmetry axis. If the disturbance speed is increased so it slightly exceeds the Alfven velocity, intermediate shocks are formed near the symmetry axis that merge continuously with fast shocks away from the symmetry axis. The authors use results from the MHD Rankine-Hugoniot equations to confirm the numerical results and demonstrate how intermediate shocks must be present in the flow field. The major general result of this study is to demonstrate the importance of considering the global configuration and, in particular, cross-flow (perpendicular to the velocity) interactions in studying wave propagation. A multi-dimensional analysis is essential in order to allow different regions of the flow field to communicate and interact with each other.

IV. Driving Mechanisms

A. Observations

One of the primary results derived from several data sets in recent years is the fact that the flare impulsive phase follows the CME onset by a relatively long time period. The time delay is long enough that any energy release in the flare cannot be solely responsible for driving the CME outward. This was convincingly demonstrated by combining data from the hard X-ray imaging spectrometer (HXIS) on SMM with C/P coronagraph data (Simnett and Harrison, 1985; Harrison, 1986). The general results from this study are shown in the schematic in Fig. 5, where the line labeled CME locates the leading edge of the bright CME loop. Extrapolation of the CME trajectory back to the surface with no acceleration shows that the CME onset coincides with a weak precursor some tens of minutes prior to the flare impulsive phase. In addition to providing the time sequence of events, the imaging capability of the X-ray instrument locates the flare site in one of the footpoints of the large magnetic arch that brightens in X-rays as the precursor. This asymmetry also argues against the flare as the driving mechanism.

Other simultaneous data sets have been used to determine the possible role of the eruptive prominence (filament) in the CME phenomena. Kahler *et al.* (1988) used Hα data from Big Bear Observatory to locate the filament and hard X-ray emission from instruments on the ISEE spacecraft for the flare impulsive phase. They were able to show that the filament eruption begins several minutes before the impulsive phase and that there is no appreciable change in the filament motion during the flare. They concluded that the filament eruption was not driven as a result of any pressure pulse associated with the impulsive flare, thereby corroborating the relatively passive role of the flare in driving CMEs as found by Harrison and others.

Additional studies combining coronagraph and Hα data have examined the relative outward motion of CMEs and erupting filaments (Wagner, 1983; Illing and Hundhausen, 1986). The main results are that the CME and prominence begin moving outward at approximately the same time although the CME (bright loop) velocity exceeds that of the erupting prominence.

The general conclusion from the above studies is that observations do not support either the flare impulsive phase or the eruptive prominence as likely candidates for propelling CMEs outward. On the other hand, the observations do support the interpretation that at least the initiating agent for the driver may be a loss of equilibrium in the large-scale (global) magnetic field configuration. That is, the global field may slowly be stressed to the extent that it can no longer remain in equilibrium. In this picture, the CME, flare impulsive phase and eruptive prominence are all secondary effects resulting from the nonlinear evolution as the corona adjusts to a new global equilibrium. The nature of the physical interactions occurring in this nonlinear stage and the means by which they produce the observable consequences have yet to be studied, for the most part, with quantitative analyses.

Some support for the gradual build up to a loss of equilibrium hypothesis can be seen in synoptic maps derived from SMM coronagraph data. Daily-averaged observations at a fixed height above the limb are shown in Figure 6. Noting that time runs from right to left in this presentation, one can see several examples of a gradual broadening of the bright region over several days (say from day 310 to day 317 on the east limb) followed by an abrupt reduction in brightness. The broadening signal is due to a gradual expansion of a coronal streamer, and a CME is observed to occur on the day in which there is a sudden decrease in brightness. The obvious interpretation being that the streamer configuration is slowly stressed to the extent that it losses equilibrium and generates a

CME. The sudden disappearance of the bright signature following the CME suggests that fields have reconnected.

B. Models: Theory and Simulation

The observations reviewed above have established the spatial and temporal relation of various individual structures identified by their unique emission characteristics during a mass ejection. The different emission characteristic of the separate components naturally means that they occur for quite different physical (primarily thermodynamic) conditions. Although the magnetic field cannot be directly measured in the corona, it is generally accepted (and supported by indirect inference) to be an important, if not dominant, contribution to the CME initiation and propagation. Some of the analytic and numerical models that have been used to try understand the physical processes in these phenomena will now be discussed briefly. A common, and necessary ingredient in all models is the magnetic field.

The first numerical simulations of CMEs used a local increase in thermal pressure as the driving mechanism. Such a driver was based on the previous view that energy released during the flare impulsive phase may become available to create the CME. Although such a driver is not supported by the observations, as discussed above, studies using thermal drivers have been useful in studying the coronal response to an outward propagating disturbance. They have clearly demonstrated the significant influence of the physical conditions (magnetic configuration, flow velocity, thermodynamics) in the ambient corona on the CME. In fact, all of the observed characteristics of looplike CMEs discussed by Sime *et al.*, (1984) have been reproduced by simulations of a CME initiated by a thermal driver at the base of a coronal streamer in a heated corona (Steinolfson and Hundhausen, 1988a). Since the driver used in this simulation is clearly inadequate, the suggestion is that the

initial state of the corona is the primary factor in determining the brightness signature rather than the details of the driver.

The only studies using magnetic, rather than the above thermal, forces to drive CMEs have been simplified to the extend that they are limited to a single radial dimension and neglect interactions with the surrounding atmosphere (e.g.; Mouschovias and Poland, 1978; Anzer, 1978). The only contribution of such models is to demonstrate that radially unbalanced magnetic pressure and force can, for not unreasonable parametric values, produce an outward motion comparable to that observed in some CMEs.

The use of a localized thermal or magnetic driver to propel CMEs outward provides useful information about CME propagation in the corona. However, as mentioned previously, observations suggest that the entire phenomena is initiated by a loss of equilibrium in the global magnetic field following a comparatively slow evolution to a highly stressed state. One way in which such a nonpotential stressed state could arise is as a result of slow evolution of the coronal field due to photospheric motion of the footpoints. With continued photospheric motion the global field may reach a configuration beyond which it no longer has an equilibrium solution and hence begins to move much more rapidly. The response of the coronal field to photospheric shear motion has been studied analytically for many years (e.g.: Low, 1982; Birn and Schindler, 1981). These simplified models generally consider only force-free magnetic field evolution and neglect the interaction of the field with the coronal motion and thermodynamics. The usual approach is to find sequences of equilibrium solutions for a given form of a generating function relating the sheared field to a parameter α. As α is changed monotonically, a value is reached beyond which there is no equilibrium solution, and this point is then identified with the onset of a more rapid evolution. The major problem with these pseudo-evolution studies is that the solutions do not uniquely relate to footpoint motion. A multiplicity of solutions for given α led

Jockers (1978) to suggest that in an actual situation the critical value of α may never be achieved. This latter view is supported by recent numerical simulations (Klimchuk *et al.*, 1988; Biskamp and Welter, 1988). The study by Klimchuk *et al.* also assumed force-free evolution as in the analytic studies. It should be pointed out that their results only demonstrate that at least one equilibrium solution can be found beyond the critical shear. A more complete study would consider all possible sheared states beyond the critical value. Biskamp and Welter include more physics in their model (magnetic field-flow interaction) and, therefore, the analytic results for force-free evolution may not apply. In addition to showing the continued slow evolution of a single magnetic arcade beyond analytically predicted stable limits, Biskamp and Welter showed that shearing of at least 3 adjacent arcades was necessary to give rise to an ejection. It remains to develop such models to the extent that their predictions can be compared to coronagraph signatures.

V. Discussion

The potential role of waves in the CME has been clarified to some extent by numerical simulations. More convincing evidence of their presence and contribution would be provided if brightness signatures attributed solely to the waves could be identified in the observations. We have already mentioned that the disturbance of adjacent structures seen in the data is probably due to a fast-mode MHD wave, which produces an undetectable density rise. Of more current interest, then, would be to clarify their effect nearer and perhaps ahead of the bright CME loop. For most typical CME velocities, it was shown how an expansion wave preceeds the slow (or intermediate) MHD shock near the outer edge of the central portion of the loop. Such as expansion would produce a density depression and reduction in brightness ahead of the bright shock compression. In addition, if the compression near the outer leading edge is produced by a concave-outward slow shock

or by an intermediate shock, the outer central portion of the loop would be depressed. Such flat tops have been seen in some CMEs. However, a more quantitative and thorough comparison with the data is needed to clearly establish the role of the MHD shocks.

Most of the available observational evidence implies that a loss of equilibrium in the global magnetic field initiates the complex phenomena collectively referred to as a CME. The precise nature of the driving mechanism and, more specifically, how an unstable, stressed magnetic configuration nonlinearly evolves to a stable configuration at lower energy is poorly understood. Intimately involved with this issue is the question of how the field loses equilibrium, and whether it occurs primarily in the open-field region of a streamer or in the underlying closed field, which tends to be more highly stressed. Simplified analytic studies will continue to provide useful guides in determining equilibrium magnetic field configurations. Unfortunately, the limited physics that can be included in the analytic models raises the question of how well they apply to a realistic corona. We mentioned above that simulations of field shear which includes the interaction of the magnetic field and velocity (non force-free field) do not indicate the presence of a critical shear value as predicted by analytic theory for a force-free field. It appears that any real progress in understanding the nature of the loss of equilibrium and the CME driver will come primarily from continued use of numerical simulations. Additional driving mechanisms, such as emerging flux due to magnetic buoyancy (the nonlinear Parker instability), and energy conversion by field reconnection should also receive continued theoretical and numerical study.

Observations with more detailed spatial and temporal resolution are also crucial to improving our understanding of the CME and associated phenomena. The observations suggested for the Max '91 program should help clarify the role of the flare and eruptive prominence. The important contribution of the magnetic field also indicates the neces-

sity for more sensitive magnetograph observations. Finally, continued observations with the instrument in which the CME was originally identified (white-light coronagraph) are necessary to continue the progress achieved to date.

Acknowledgemnts

The author thanks the High Altitude Observatory of the National Center for Atmospheric Research, which is sponsored by the National Science Foundation, for support as a visiting scientist during most of the period in which this manuscript was prepared. The work was also partially supported by NASA Guest Investigator Grant NAG5-1092 and NASA Grant NAGW-1324.

Figure Captions

1. A representative loop-like CME observed by the SMM coronagraph. This image was obtained on April 14, 1980 and shows the characteristic three-part structure of a bright leading loop followed by a dark cavity containing a second bright structure. From Hundhausen (1984a).

2. A schematic illustrating the corona prior to a CME (a) and the relation of various phenomena during the ejection (b).

3. The speculated geometry of the fast (a) and slow (b) MHD shocks generated as part of the CME. From Hundhausen *et al.* (1987).

4. Slow shock geometry produced in MHD simulations using a vertical magnetic field and a thermal driver. From Steinolfson and Hundhausen (1988b).

5. Schematic of temporal and spatial relation between the precursor, flare impulsive phase, and the CME bright loop. From Harrison (1986).

6. Synoptic map produced from SMM coronagraph obsevations showing the daily-averaged brightness at 2.8 solar radii and at both limbs. Unpublished results supplied by A. J. Hundhausen.

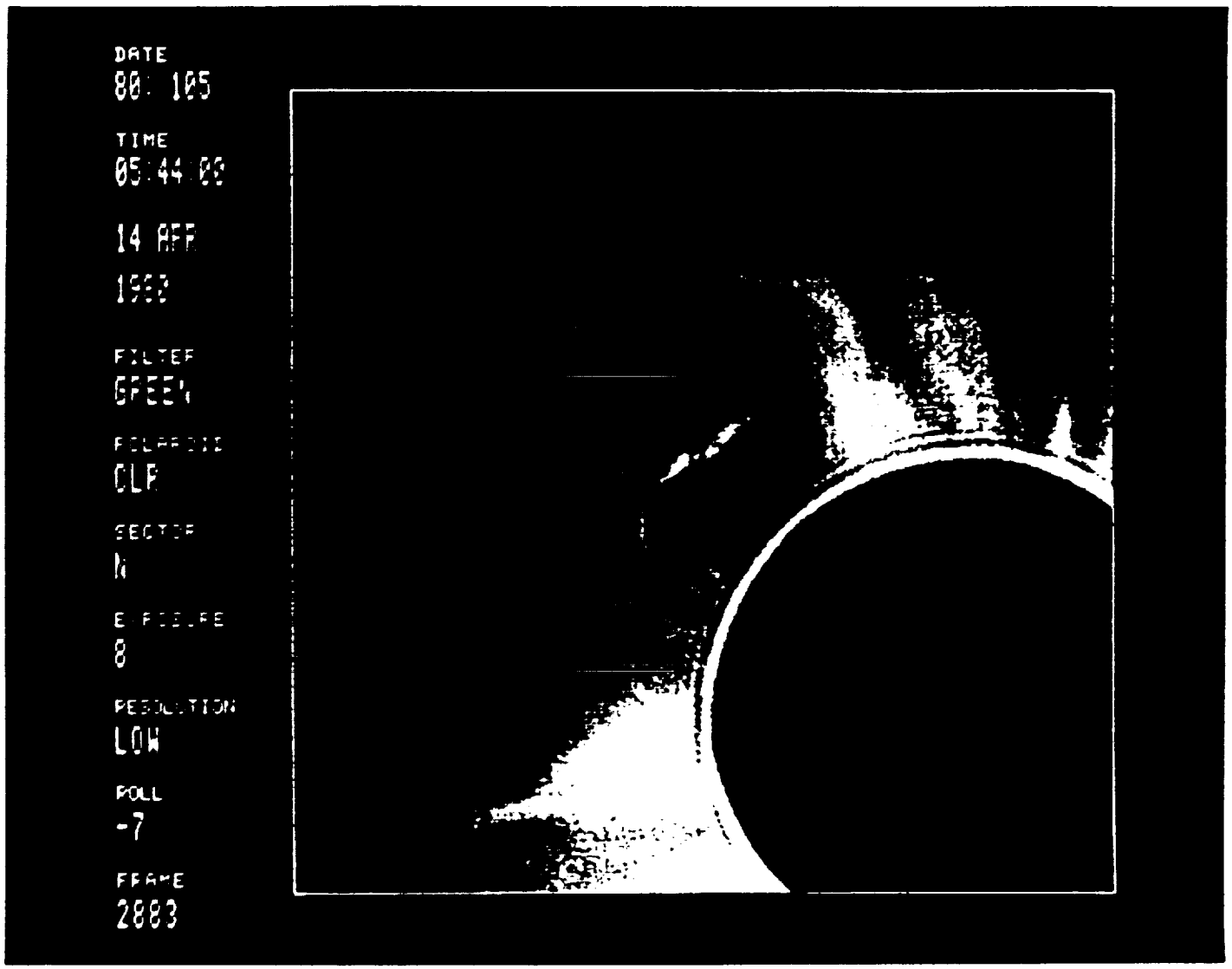

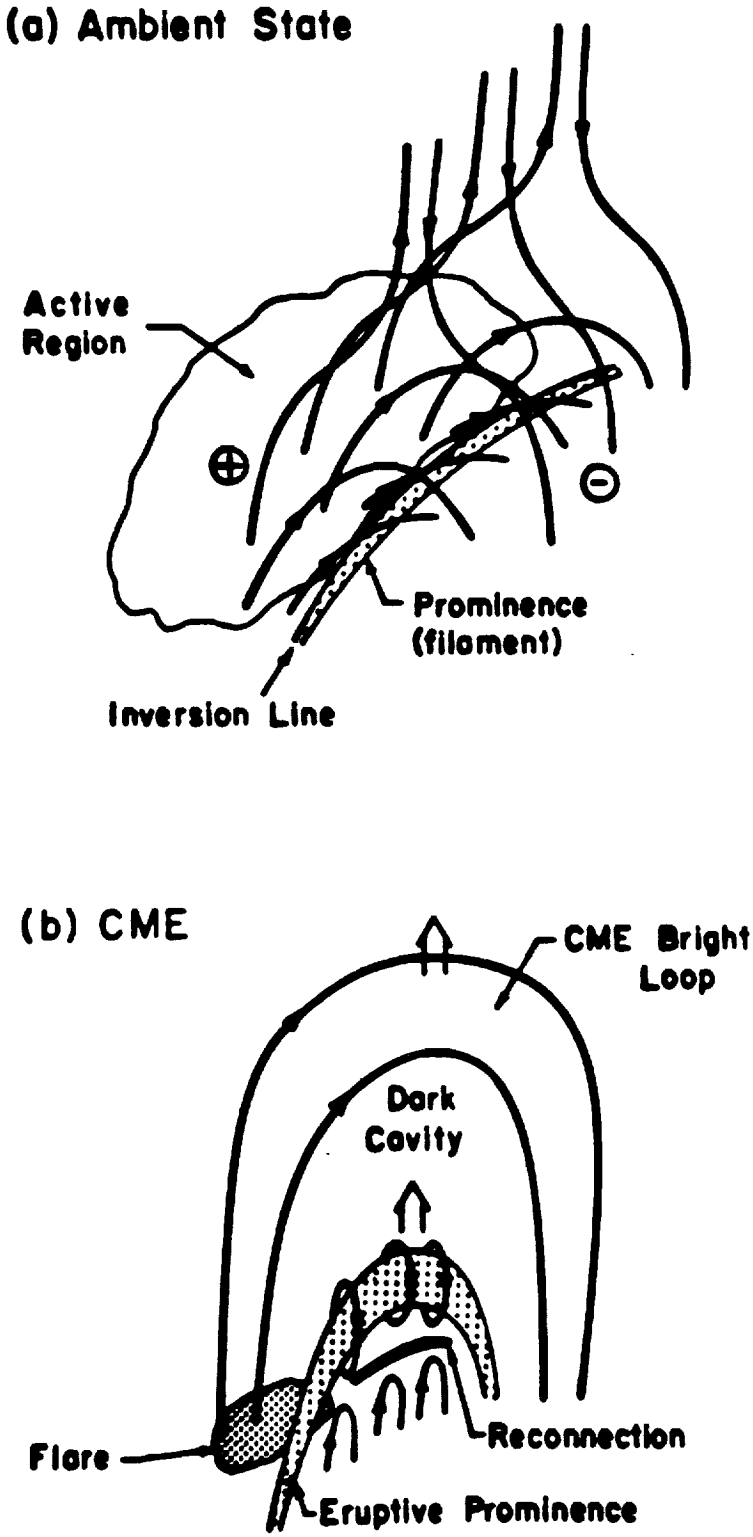
(a) Ambient State
Active Region
⊕
⊖
Prominence (filament)
Inversion Line
(b) CME
CME Bright Loop
Dark Cavity
Flare
Reconnection
Eruptive Prominence

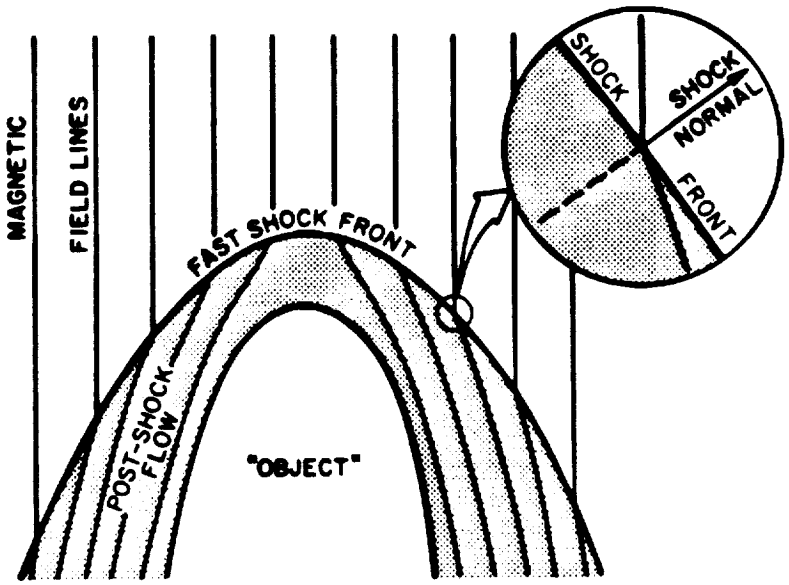

a. Spatial Configuration of a "Fast" Bow Shock

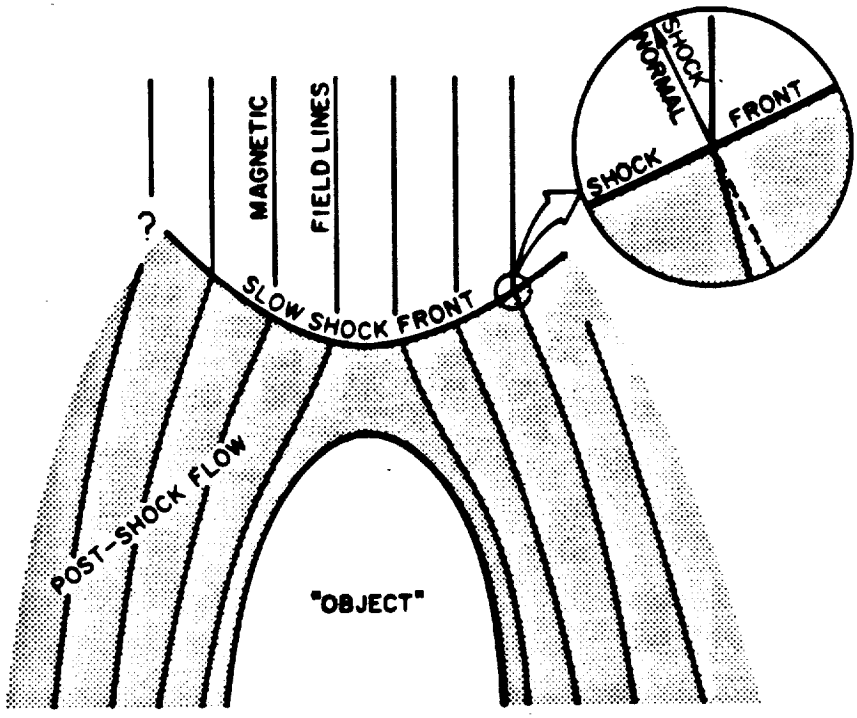

b. Proposed Spatial Configuration of a "Slow" Bow Shock

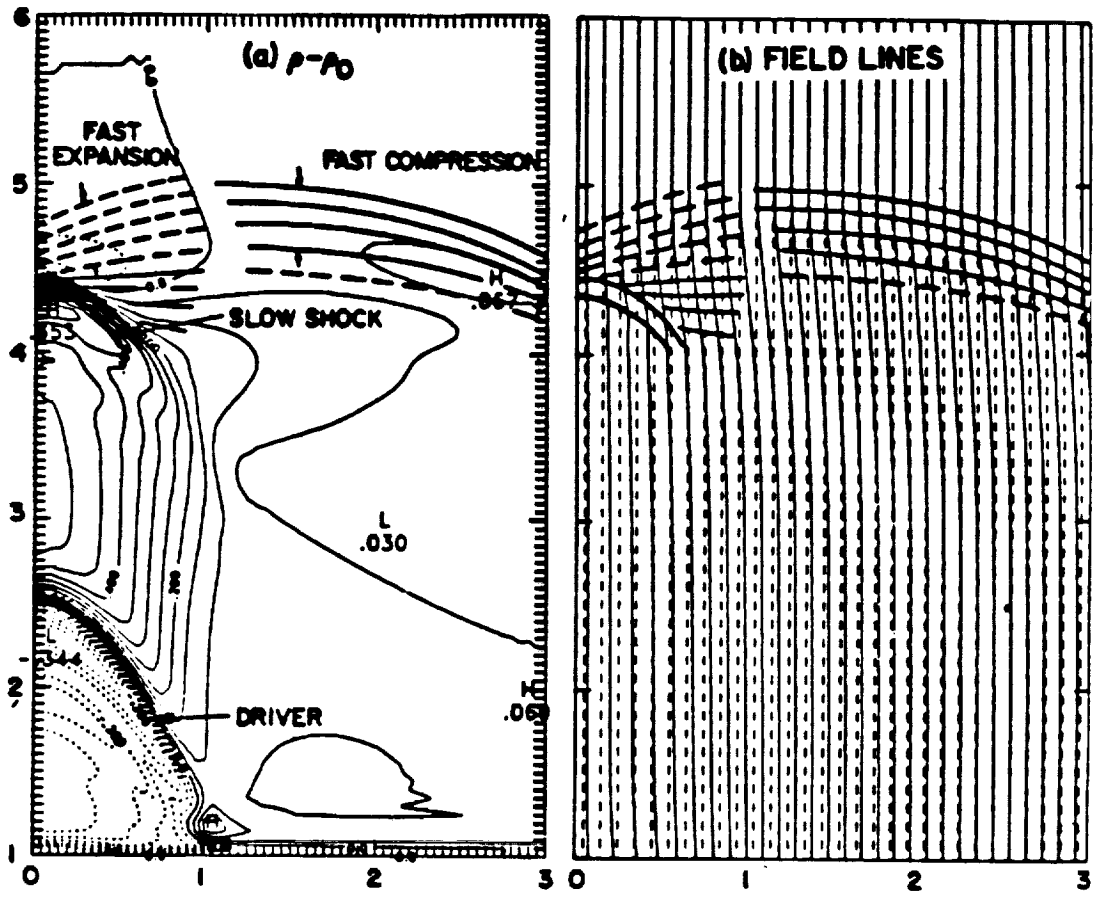

3.5–5.5 keV
X-RAY INTENSITY
Flare
CME
Precursor
CORONAL MASS EJECTION
ALTITUDE
TIME →
Flare - Site
Precursor Arch
CME
Solar
Limb
~10^5 km

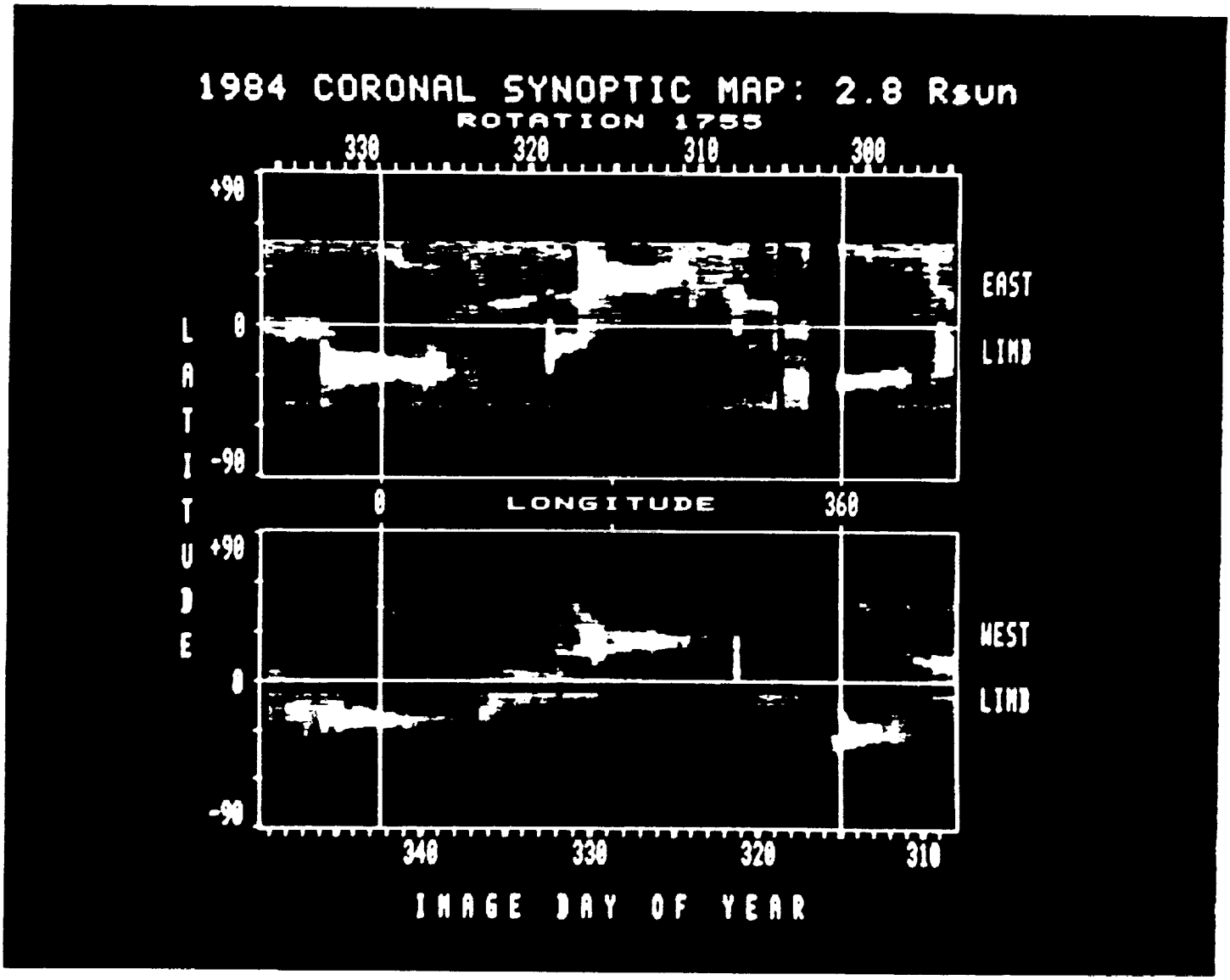

References

Birn, J., and K. Schindler, Two ribbon flares: Magnetostatic equilibria, in *Solar Flare Magnetohydrodynamics,* ed. by E.R. Priest, Gordon and Breach, New York, 337, 1981.

Biskamp, D., and H. Welter, Magnetic arcade evolution and instability, *Solar Phys.,* Submitted, 1988.

Dryer, M., S.T. Wu, R.S. Steinolfson, and R.M. Wilson, Magnetohydrodynamic models of coronal transients in the meridional plane. II. Simulation of the coronal transient of 1973 August 21, *Astrophys. J., 227,* 1059, 1979.

Fisher, R.R., and A.I. Poland, Coronal activity below 2 R_o: 1980 February 15-17, *Astrophys. J., 246,* 1004, 1981.

Gosling, J.T., E. Hildner, R.M. MacQueen, R.H. Munro, A.I. Poland, and C.L. Ross, The speeds of coronal mass ejection events, *Solar Phys., 48,* 389, 1976.

Harrison, R.A., Solar coronal mass ejections and flares, *Astron. Astrophys., 162,* 283, 1986.

Harrison, R.A., E. Hildner, A.J. Hundhausen, G.M. Simnett and D.G. Sime, The launch of coronal mass ejections: Results from the coronal mass ejection onset program, *J. Geophys. Res.,* submitted, 1988.

Howard, R.A., N.R. Sheeley, Jr., M.J. Koomen, and D.J. Michels, The statistical properties of coronal mass ejections during 1979-1981, *Adv. Space Res., 4,* 307, 1984.

Howard, R.A., N.R. Sheeley, Jr., M.J. Koomen, and D.J. Michels, Coronal mass ejections: 1979-1981, *J. Geophys. Res., 90,* 8173, 1985.

Hundhausen, A.J., The origin and propagation of coronal mass ejections, in *Proceedings of the Sixth International Solar Wind Conference*, ed. by V.J. Pizzo, T.E. Holzer and D.G. Sime, 181, NCAR/TN-306, 1988.

Hundhausen, A.J., C.B. Sawyer, L. House, R.M.E. Illing, and W.J. Wagner, Coronal mass ejections observed during the solar maximum mission: latitude distribution and rate of occurrence. *J. Geophys. Res., 89*, 2639, 1984a.

Hundhausen, A.J., et al., Coronal transients and their interplanetary effects, in *Solar Terrestrial Physics: Present and Future,* ed. by D.M. Butler and K. Papadopoulos, p. 6-1, NASA Ref. Publ. 1120, 1984b.

Hundhausen, A.J., T.E. Holzer, and B.C. Low, Do slow shocks precede some coronal mass ejections?, *J. Geophys. Res., 92*, 173, 1987.

Illing, R.M.E., and A.J. Hundhausen, Disruption of a coronal streamer by an eruptive prominence and coronal mass ejection, *J. Geophys. Res., 91,* 10,951, 1986.

Jockers, K., Bifurcation of force-free solar magnetic fields: A numerical approach. *Solar Phys., 56,* 37, 1978.

Jackson, B.V., and C. Leinert, Helios images of solar mass ejections, *J. Geophys. Res., 90,* 10, 759, 1985.

Kahler, S., Coronal mass ejections, *Rev. Geophys., 25,* 663, 1987.

Kahler, S., Observations of coronal mass ejections near the sun, in *Proceedings of the Sixth International Solar Wind Conference*, ed. by V.J. Pizzo, T.E. Holzer and D.G. Sime, 181, NCAR/TN-306, 1988.

Kahler, S.W., R.L. Moore, S.R. Kane, and H. Zirin, Filament eruptions and the impulsive

phase of solar flares, *Astrophys. J., 328*, 824, 1988.

Klimchuk, J.A., P.A. Sturrock and W.-H. Yang, Coronal magnetic fields produced by photospheric shear, *Astrophys. J.,* submitted, 1988.

Kopp, R.A., and G.W. Pneuman, Magnetic reconnection in the corona and the loop prominence phenomenon, *Solar Phys., 50,* 85, 1976.

Low, B.C., Nonlinear force-free magnetic fields, *Rev. Geophys. Space Phys., 20*, 145, 1982.

MacQueen, R.M., Coronal mass ejections: acceleration and surface associations, *Solar Phys., 95,* 359, 1985.

Mouschovias, T. Ch., and A.I. Poland, Expansion and broadening of coronal loop transients: A theoretical explanation, *Astrophys. J., 220,* 675, 1978.

Munro, R.H., J.T. Gosling, E. Hildner, R.M. MacQueen, A.I. Poland, and C.L. Ross, The association of coronal mass ejection transients with other forms of solar activity, *Solar Phys., 61,* 201, 1979.

Sheeley, N.R., Jr., R.A. Howard, D.J. Michels, and M.J. Koomen, Solar observations with a new earth-orbiting coronagraph, in *Solar and Interplanetary Dynamics,* ed. by M. Dryer and E. Tandberg-Hanssen, D. Reidel, Hingham, MA, 55, 1980.

Sime, D.G., and A.J. Hundhausen, The coronal mass ejection of July 6, 1980: A candidate for interpretation as a coronal shock wave, *J. Geophys. Res., 92,* 1049, 1987.

Sime, D.G., R.M. MacQueen, and A.J. Hundhausen, Density distribution in loop-like coronal transients: A comparison of observations and a theoretical model, *J. Geophys. Res., 89*, 2113, 1984.

Simnett, G.M., and R.A. Harrison, The relationship between coronal mass ejections and solar flares, *Adv. Space Res., 4,* 279, 1984.

Steinolfson, R.S., Theories of shock formation in the solar atmosphere, in *Collisionless Shocks in the Heliosphere: Reviews of Current Research,* ed. by B.T. Tsurutani and R.G. Stone, American Geophysical Union, Washington, 1, 1985.

Steinolfson, R.S., Driving mechanisms for coronal mass ejections, in *Outstanding Problems in Solar System Plasma Physics: Theory and Instrumentation,* ed. by J. Birch and J. Hunter, in press, 1988.

Steinolfson, R.S., and A.J. Hundhausen, Density and white-light brightness in loop-like coronal mass ejections: Temporal evolution, *J. Geophys. Res.*, in press, 1988a.

Steinolfson, R.S., and A.J. Hundhausen, Waves in low-beta plasmas: Slow shocks, *J. Geophys. Res.,* in press, 1988b.

Steinolfson, R.S., and A.J. Hundhausen, MHD intermediate shocks in coronal mass ejections, *J. Geophys. Res.,* ~~in press~~ submitted, 1988c.

Tousey, R., The solar corona, in *Space Research XIII,* ed. by M.J. Rycroft and S.K. Runcorn, Akademie-Verlage, Berlin, 713, 1973.

Wagner, W.J., SERF studies of mass motions arising in flares, *Adv. Space Res., 2,* 203, 1983.

Wagner, W.J., Coronal mass ejections, *Ann. Rev. Astron. Astrophys., 22,* 267, 1984.

Webb D.F., and A.J. Hundhausen, Activity associated with the solar origin of coronal mass ejections, *Solar Phys., 108,* 383, 1987.